BIOMASS AND BIOENERGY XXX (2014) 1–10

Available online at www.sciencedirect.com

ScienceDirect

http://www.elsevier.com/locate/biombioe

New approaches to measuring biochar density and porosity

Catherine E. Brewer [a,b,*], *Victoria J. Chuang* [a], *Caroline A. Masiello* [a,**], *Helge Gonnermann* [a], *Xiaodong Gao* [a], *Brandon Dugan* [a], *Laura E. Driver* [c], *Pietro Panzacchi* [d,e], *Kyriacos Zygourakis* [b], *Christian A. Davies* [e]

[a] *Department of Earth Science, Rice University, 6100 Main St. MS 126, Houston, TX 77005, USA*
[b] *Department of Chemical and Biomolecular Engineering, Rice University, 6100 Main St. MS 362, Houston, TX 77005, USA*
[c] *Cinco Ranch High School, Katy Independent School District, Katy, TX 77494, USA*
[d] *Department of Agricultural Sciences-DipSA, University of Bologna, Viale Fanin 44, Bologna 40127, Italy*
[e] *Shell International Exploration and Production Inc., Shell Technology Center Houston, P.O. Box 4685, 3333 Highway 6 South, Houston, TX 77251, USA*

ARTICLE INFO

Article history:
Received 4 October 2013
Received in revised form
25 March 2014
Accepted 26 March 2014
Available online xxx

Keywords:
Biochar
Skeletal density
Envelope density
Pore volume
Gas sorption analysis
Mercury porosimetry

ABSTRACT

It is clear that the density and porosity of biochar will impact its mobility in the environment, its interaction with the soil hydrologic cycle, and its suitability as an ecological niche for soil microorganisms. However, the wide range of biochar pore sizes complicates biochar porosity characterization, making it challenging to find methods appropriate to connect the fundamental physical properties of density and porosity to environmental outcomes. Here, we report the use of two fast, simple density measurement techniques to characterize biochar density and porosity. We measured biochar skeletal density by helium pycnometry and envelope density by displacement of a dry granular suspension. We found that biochar skeletal density ranged from 1.34 g cm^{-3} to 1.96 g cm^{-3}, and increased with pyrolysis temperature. Biochar envelope density ranged from 0.25 g cm^{-3} to 0.60 g cm^{-3}, and was higher for wood biochars than grass biochars—a difference we attribute to plant cell structures preserved during pyrolysis. We compared the pore volumes measured by pycnometry with those measured by nitrogen gas sorption and mercury porosimetry. We show that biochar pore volumes measured by pycnometry are comparable to the values obtained by mercury porosimetry, the current benchmark method. We also show that the majority of biochar pore volume is in macropores, and thus, is not measured by gas sorption analysis. These fast, simple techniques can now be used to study the relationship between biochar's physical properties and its environmental behaviors.

* *Corresponding author*. Department of Chemical Engineering, New Mexico State University, P.O. Box 30001 MSC 3805, Las Cruces, NM 88003, USA. Tel.: +52 575 646 8637; fax: +52 575 646 7706.
** *Corresponding author*. Tel.: +1 713 348 5234; fax: +1 713 348 5214.
E-mail addresses: cbrewer@nmsu.edu (C.E. Brewer), masiello@rice.edu (C.A. Masiello).

http://dx.doi.org/10.1016/j.biombioe.2014.03.059
0961-9534/

1. Introduction

Charcoal enters the environment as a natural byproduct of fire, where it is a component of the larger black carbon pool that also includes soot. When charcoal enters soils through intentional human amendment to sequester carbon and increase crop productivity, it is called biochar. If the adoption of biochar as a climate change mitigation option is to be implemented at any significant scale [1], we must understand how the natural environment is affected by the fate, transport, and ecosystem services [2] of this biochar material.

While it has been possible to characterize the biological and chemical controls on biochar environmental residence times and ecosystem services [3], we know much less about the physical processes that determine the transport and interactions of biochar within the environment. A first step in understanding these two topics is a description of biochar physical properties beyond particle size. Density and porosity are fundamental physical properties that control how biochar moves through the landscape and how it interacts with water to alter soil hydrologic processes, particularly plant-available water holding capacity [4]. These properties likely also impact biochar's capacity to act as an ecological niche, for example, by providing growing space for microbes and shelter for mycorrhizal fungi from predators [5], and subsequently affecting the accessibility of substrates and nutrients in important biogeochemical cycles mediated by these soil microorganisms.

Density and porosity almost certainly play a role in biochar transport within the soil environment because materials with bulk densities less than water (<1 g cm^{-3}) will float. There is evidence that under some circumstances, black carbon in general and biochar specifically can be transported within soils. For example, Rumpel et al. observed preferential erosion of black carbon in steeply sloped soils (46% slope) in Laos which had been subjected to slash-and-burn agriculture [6]. The concentration of black carbon was 2.2 times higher in the eroded sediments than in the corresponding bulk soils, a result that the authors attributed to the tendency of black carbon to float. In a rainfall simulator experiment on a 1% slope soil with added black carbon, Rumpel et al. also showed that up to 55% (550 g kg^{-1}) of the black carbon was transported horizontally, a result which was again attributed to charcoal's ability to float under some hydrologic conditions [7]. Similar horizontal movement was shown in a biochar amendment where the applied biochar had a traceable isotopic signal. Through subtraction, Major et al. estimated that 20%–53% (200 g kg^{-1} to 530 g kg^{-1}) of applied biochar was lost through surface runoff over a 2-year period following tillage of biochar into a soil with no visible inclination (slope <2%) [8]. Higher erosion rates of black carbon, relative to other forms of terrestrial organic matter, also have implications for the composition of fluvial organic matter and long-term carbon sinks in marine sediments [9–11]. These examples highlight the importance of understanding the environmental impacts of the physical, in addition to the chemical, characteristics of biochar.

An accurate characterization of biochar pore structure and pore size distribution is challenging, because the pore sizes of biochars range over at least five orders of magnitude, from sub-nanometer slit-shaped pores that correspond to spaces between graphite-like layers of flat aromatic carbon clusters [12–14], to pores on the order of tens of micrometers from partially preserved cellular structures [15,16]. There is no single technique that can measure pore volume precisely across these scales, and as a result, effective biochar porosity characterization has been elusive.

Gas sorption methods have been popular for characterizing the porosity of carbon materials due to their relative ease of use and demonstrated relationship to chemical sorbate–sorbent interactions [17]. The most common methods involve carbon dioxide adsorption to characterize biochar pores that are smaller than 2 nm (sub-micropores) and nitrogen adsorption with BET analysis to characterize pores in the <2 nm–50 nm range (micro- and meso-pores). These adsorption methods do not, however, provide any information about pores larger than mesopore size (macropores), which have been shown in electron microscopy images to be present in many biochar samples [12,18–23].

Mercury porosimetry can be used to characterize pores with openings from a few nanometers to a few hundred micrometers in diameter [24]. Previous work has demonstrated that mercury porosimetry detects more biochar pore volume than gas sorption does [25]. The drawbacks of mercury porosimetry, however, include the risk of crushing the sample with the high pressures required for analysis, thereby introducing inaccuracies in the porosity measurements, and its inability to distinguish between inter-particle and intra-particle porosity, especially for powdered samples. There are further limitations with safety and handling mercury, and the destructive nature of the analysis method. Another difference of mercury porosimetry is that it determines the diameter of the pore throat, not the actual pore size [24]. Finally, the fact that biochars are granular materials with highly variable surface chemistry complicates the measurement of the contact angle between mercury and the biochar surfaces, and the relationship between pressure and pore throat size is directly dependent on contact angle [24].

Stereological methods based on sectioning, image analysis, and 3-D reconstruction techniques have been used to visualize the largest pores (typically >1 μm) of carbonaceous materials [26,27], but are not quantitative. Techniques like scanning electron microscopy (SEM) are frequently used in biochar characterization studies [12,18,25], and are excellent at detecting biochar macropores. However, microscopy and computerized tomography (CT) face challenges including selection of representative samples and viewing orientations, definition of edges between solid and pore, and development of image analysis protocols to quantify porosity [15].

Here we report a novel approach to measure the total pore volume of biochars using two forms of density measurement: skeletal and envelope density. Both techniques measure the volume of a known mass by a displacement technique. In the case of skeletal density (ρ_s), the displaced material is helium gas; in the case of envelope density (ρ_e), the displaced material is a micro-granular suspension. Combined, these two density measurements can be used to calculate a sample's porosity. We assess biochar porosity variation across two feedstocks, a range of pyrolysis temperatures, and two reactor conditions in

Please cite this article in press as: Brewer CE, et al., New approaches to measuring biochar density and porosity, Biomass and Bioenergy (2014), http://dx.doi.org/10.1016/j.biombioe.2014.03.059

order to connect biochar production conditions with biochar physical properties.

2. Materials and methods

2.1. Biochar production

Miscanthus grass (*Miscanthus giganteus*, a sterile hybrid of *Miscanthus sinensis* and *Miscanthus sacchariflorus*) for intermediate-slow pyrolysis was acquired from a farm in Groningen province, the Netherlands (53°13′00″ N, 6°34′00″ E). The mixed-age miscanthus was harvested from all above-ground biomass at senescence (March/April) and supplied to the commercial market. The miscanthus was chipped to approximately 20 mm–40 mm and stored dry (average moisture content of 110 g kg^{-1} on a wet biomass basis) in sealed containers prior to pyrolysis; this particle size was selected to accommodate the auger pyrolyzer reactor design (Section 2.1.2) [28]. Mesquite wood (*Prosopis glandulosa*) chips were purchased from a local grocery store (H-E-B, Houston, TX; H-E-B is headquartered in San Antonio, TX) and stored as received (dry) in sealed containers in the lab. The mesquite wood was ground and sieved to between 4.75 mm and 3.35 mm prior to pyrolysis, a range optimal for the envelope density measurement.

2.1.1. Slow pyrolysis biochars

Slow pyrolysis biochars were produced in a fixed bed reactor as described in Kinney et al. [29]. Biomass was placed in a stainless steel crucible, which was then plugged with ceramic wool, capped with a ceramic bowl, and buried in fine-grained quartz sand inside a larger, open-top stainless steel crucible. This reactor system was heated in a muffle furnace at 5–6 K min^{-1} up to the reaction temperature and held at that temperature for 4 h. A summary of biochars produced and biochar yields is shown in Table 1. Slow pyrolysis biochars are indicated by the letter "S" followed by their feedstock and final pyrolysis temperature (e.g. S Grass 400).

2.1.2. Intermediate pyrolysis biochars

Miscanthus grass "intermediate" pyrolysis biochars were produced using an auger pyrolyzer by BTG Biomass Technology Group B.V. (Enschede, the Netherlands). The biomass was manually fed into an initial auger reactor and heated to temperatures around 120 °C–130 °C to reduce moisture content. After passing through the initial auger reactor, the biomass was pyrolyzed in a second auger reactor at different final pyrolysis temperatures (350 °C, 360 °C, 370 °C, 400 °C, 425 °C, and 450 °C). Both reactors consisted of two concentric tubes. The inner tube holds a conveyor while the outer shell acts as the heating jacket. Both reactors are heated by combusting pyrolysis process residual vapors and gases with air at 850 °C and passing the hot combustion gases through the outer reactor shell. Residence times in the second auger reactor at final pyrolysis temperatures averaged 14.7 (±0.4) min (yields are reported in Table 1). These biochars are described as intermediate because the target heating rate is higher and the particle residence time shorter than are typical for slow pyrolysis, yet neither condition nor the resulting product yields could be considered indicative of fast pyrolysis. Intermediate pyrolysis biochars are indicated by the letter "I" followed by their feedstock and final pyrolysis temperature (e.g. I Grass 400).

Table 1 – Yield, composition and elemental molar ratios of grass and wood biochars and feedstocks. Grass intermediate pyrolysis char yields are reported on a wet basis (11% w/w moisture). Moisture reported on a wet basis; all other values reported on a dry basis. Oxygen content determined by difference.

Sample ID	Yield	Moisture	Ash	C	H	N	O	H:C	O:C
	g kg^{-1}								
S Grass 350	408	30	49	669	38	7	238	0.67	0.27
S Grass 400	349	33	54	698	34	7	208	0.58	0.22
S Grass 450	304	31	65	728	29	6	172	0.48	0.18
S Grass 550	283	0	66	818	21	5	90	0.31	0.08
S Grass 600	271	0	64	835	16	5	80	0.23	0.07
S Grass 700	240	0	69	842	8	6	75	0.12	0.07
I Grass 350	700	23	18	514	54	5	409	1.26	0.60
I Grass 360	730	22	32	515	59	2	393	1.37	0.57
I Grass 370	400	25	49	676	51	5	219	0.90	0.24
I Grass 400	370	29	51	688	44	7	211	0.76	0.23
I Grass 425	330	31	54	701	45	5	196	0.76	0.21
I Grass 450	310	38	53	680	40	8	220	0.70	0.24
S Wood 300	620	30	29	581	43	5	343	0.89	0.44
S Wood 350	505	37	27	700	38	7	228	0.65	0.24
S Wood 400	430	31	33	719	35	9	205	0.58	0.21
S Wood 450	395	36	44	748	31	10	167	0.49	0.17
S Wood 550	342	29	61	798	24	13	104	0.36	0.10
S Wood 600	326	30	67	802	19	11	101	0.29	0.09
S Wood 700	299	43	54	843	11	7	85	0.15	0.08
Miscanthus Grass		57	21	437	62	7	473	1.70	0.81
Mesquite Wood		46	16	468	62	4	450	1.58	0.72

Please cite this article in press as: Brewer CE, et al., New approaches to measuring biochar density and porosity, Biomass and Bioenergy (2014), http://dx.doi.org/10.1016/j.biombioe.2014.03.059

2.2. Basic biochar characterization

Moisture and ash content of the feedstocks were determined in duplicate using the laboratory analytical procedures developed by the National Renewable Energy Laboratory for biomass [30,31]. Moisture and ash content of the biochars were measured in duplicate according to ASTM D1762-84 [32]. Carbon, hydrogen and nitrogen contents of the biochars and feedstocks were measured in triplicate by combustion using an ECS4010 elemental analyzer (Costech, Valencia, CA). Brunauer–Emmett–Teller (BET) surface area, Dubinin-Radushkevich (DR) micropore volume, and total micro- and meso-pore volume of the biochars were measured at least in duplicate by nitrogen gas sorption at 77 K using an Autosorb-3b gas sorption analyzer (Quantachrome Instruments, Boynton Beach, FL). Samples were vacuum degassed overnight at 250 °C prior to analysis. Total (gas sorption measurable) pore volume was determined as the cumulative volume at $P/P_0 = 0.995$ on the adsorption curve of the isotherm.

2.3. Skeletal density

Skeletal density is the sample mass divided by the sample skeletal volume, where skeletal volume is the volume occupied by the solid sample (and any pores not accessible to the analysis gas). For this study, we measured biochar skeletal volume by helium pycnometry using an AccuPyc 1340 fitted with a 1 cm^3 chamber (Micromeritics, Norcross, GA). The AccuPyc measures the skeletal volume of the sample by detecting the change in pressure due to the volume of helium that is displaced by the sample within the sealed and pressure-equilibrated chamber. It is assumed that helium atoms are able to penetrate all open pores within the biochar particle. The variability of the ρ_s measurement was assessed by measuring three separate aliquots of each biochar sample. In all cases, measurement variability caused by sample heterogeneity was greater by more than an order of magnitude than the level of measurement repeatability used to define equilibrium in the analysis method (3 $mm^3\ cm^{-3}$ to 10 $mm^3\ cm^{-3}$).

2.4. Envelope density

Envelope density is the sample mass divided by the total sample volume that would be measured if an "envelope" were placed around each individual sample particle. We measured biochar envelope volume using a Geopyc 1360 Envelope Density Analyzer (Micromeritics, Norcross, GA). In this analysis, the sample is placed in a bed of DryFlo® granular medium, which is agitated and gently consolidated around the biochar particles using a piston. According to the manufacturer, DryFlo® is a non-intruding, free-flowing, dry granular medium with a particle size distribution described by 100 g kg^{-1}, 500 g kg^{-1}, and 900 g kg^{-1} of the particles being smaller than 74 μm, 125 μm, and 185 μm, respectively. Pores which are open to the particle exterior but smaller than the DryFlo® particles are included within the volume "envelope," which also includes all interior pores. Sample volume is determined by subtracting the volume of consolidated pure DryFlo® from the volume of the same consolidated DryFlo® after the sample has been added. Consolidation is achieved by rotation and vibration of the cylindrical chamber as the piston is gradually pushed into the chamber until the desired force is reached, followed by retraction and recompression. Prior to collecting data, multiple preparation compressions are used to bring the DryFlo® plus sample closer to the "equilibrium" volume.

2.4.1. Variability of envelope density measurement

Envelope density measurement involves compressing the biochar, which is friable under enough force. For this reason, we carefully analyzed the variability associated with envelope density measurements to determine optimal measurement conditions. There are three important parameters that control variability in the ρ_e measurement (besides sample heterogeneity): 1) the percent of the total volume (DryFlo® + sample) occupied by the sample, 2) the force used to consolidate the DryFlo® and sample mixture, and 3) the conversion factor used by the instrument to convert the number of piston rotations (counts) to a volume measurement. If the sample volume percentage is too low, it is difficult to accurately measure a difference between DryFlo® volume with and without sample. On the other hand, if the sample volume percentage is too high, there may not be enough DryFlo® to completely surround the sample. Achieving the desired sample volume percentage requires some trial and error for each sample because the actual sample volume percentage is only known after the analysis is complete. Higher consolidation forces increase the likelihood that DryFlo® will completely surround the sample. If the force is too high, however, the sample may be crushed and the sample's pores destroyed. A final parameter that must be constrained is the conversion factor, which accounts for how well the DryFlo® medium conforms to the unique shape distribution of the sample.

2.4.2. Protocol development for envelope density measurement

We conducted two experiments to develop the ρ_e measurement protocol. First, we used samples of a similar mesquite wood slow pyrolysis biochar made at 400 °C to identify the analysis conditions that gave the best reproducibility with the fewest runs. We conducted a partial factorial experiment of three sample volume percentages (0.15 $cm^3\ cm^{-3}$, 0.20 $cm^3\ cm^{-3}$, and 0.25 $cm^3\ cm^{-3}$ total volume) and three consolidation forces (15 N, 22 N, and 29 N) such that the relative standard deviation over four runs could be calculated for each volume percentage–force combination. We used the results of this experiment (shown in Supporting Information Tables S1 and S2, and Figures S1 and S2) to select a sample volume of 0.25 $cm^3\ cm^{-3}$, a force of 22 N, and three runs per sample, which typically gave a relative standard deviation on the ρ_e measurement of approximately 5%. Other analysis conditions included a 12.7 mm diameter chamber, a 1.6 cm^3 total volume (as per the manufacturer recommendations that the consolidated height be approximately equal to the chamber diameter), a new blank measurement for every sample, and the instrument's maximum number of compression cycles: 20 preparation cycles + 20 measurement cycles. We chose the maximum number of cycles because biochar's irregular shape and numerous particles means that more compressions are needed to arrange and rearrange the DryFlo® and sample to achieve the densest "equilibrium" volume at a given force.

Please cite this article in press as: Brewer CE, et al., New approaches to measuring biochar density and porosity, Biomass and Bioenergy (2014), http://dx.doi.org/10.1016/j.biombioe.2014.03.059

In the second experiment, we calibrated the conversion factor for the biochar measurements using non-porous angular fragments of plastic (broken plastic fork tines, Figures S3 and S4). We chose plastic fork pieces due to their similarity in size and shape to the biochar particles. We calibrated the envelope volume of the fork pieces, determined using the analysis conditions selected in the earlier experiment, against the skeletal volume of the fork pieces as determined by He pycnometry. The resulting conversion factor we used for the biochar measurements was 0.124 $cm^3\ mm^{-1}$.

2.5. Porosity

We define porosity here as the percent of the biochar particle volume not filled by solid, as calculated from the difference in densities:

$$\text{Porosity} = \left(1 - \frac{\rho_e}{\rho_s}\right) \quad (1)$$

As previously mentioned, this porosity includes all pores that are accessible from the biochar particle exterior through openings smaller than the DryFlo® granules, as well as all the pores that are inaccessible from the exterior.

2.5.1. Pore accessibility

Not all pores within a given particle are accessible from the exterior. For example, if a pore formed during pyrolysis by escaping volatiles was later plugged by condensation of tars, the measurement of skeletal and envelope volume would inadvertently include this pore volume as solid sample volume. We assessed the occurrence of blocked macropores inaccessible to helium within the biochars by measuring the skeletal densities of biochars made at 350 °C, 400 °C, and 450 °C after grinding the samples with a mortar and pestle to pass a 53 μm screen with the assumption that grinding would open inaccessible pores.

2.5.2. Mercury porosimetry

We used mercury porosimetry to measure the pore size distribution and porosity of one sample each of five of the biochars: I Grass 350, I Grass 400, I Grass 450, S Grass 450 and S Wood 450 (where I and S designate intermediate and slow pyrolysis conditions, respectively). Mercury intrusion measures porosity with the sample's bulk/envelope and absolute/skeletal volumes defined as the volume occupied by the sample when the sample chamber is filled with mercury at absolute pressures of 3.58 kPa (partial vacuum) and 414 MPa, respectively. At these pressures, mercury is theoretically able to penetrate into pore entrances of approximately 400 μm and 3 nm, respectively. Micromeritics Analytical Services performed the analysis using an AutoPore IV mercury porosimeter (Micromeritics, Norcross, GA).

3. Results and discussion

3.1. Biochar yield and composition

Biochar yield and composition varied with feedstock, temperature and pyrolysis method (Table 1). Yield decreased with increasing biochar production temperature. Grass and slow pyrolysis led to lower yields than wood and intermediate pyrolysis for biochars made at the same reactor temperature. Differences in yield and CHN content attributed to pyrolysis method were most noticeable for grass at 350 °C (I Grass 350). The relatively high H:C molar ratio and slightly brown color for the intermediate pyrolysis biochars at reactor temperatures of 350 °C and 360 °C suggest an incomplete conversion of the lignocellulose during pyrolysis (i.e. the biomass did not have enough time to reach reactor temperature). This kind of incomplete conversion due to a faster heating rate and shorter residence time has been previously described [33]. The sharp change in biochar properties between 360 °C and 370 °C can be explained by the decomposition of the majority of the cellulose in the miscanthus over this temperature range. The decomposition of cellulose occurs primary between 315 °C and 390 °C, with the highest decomposition rate occurring at 355 °C [34]. Higher yields for wood biochar could be due to a higher lignin content of mesquite wood (640 g kg^{-1}) [35] compared to miscanthus grass (100 g kg^{-1} to 300 g kg^{-1}) [36] given that lignin produces more char upon heating than hemicellulose or cellulose [37].

3.2. Biochar surface area and porosity by gas sorption

BET surface area of the slow pyrolysis biochars increased exponentially with pyrolysis temperature, from <1 $m^2\ g^{-1}$ to 317 ± 16 $m^2\ g^{-1}$ for the wood biochars and from <1 $m^2\ g^{-1}$ to 387 ± 6 $m^2\ g^{-1}$ for the grass biochars. BET surface area was low, <10 $m^2\ g^{-1}$, for all of the intermediate pyrolysis biochars (Fig. 1). The increase in surface area with temperature mirrored the increase in micropore volume (shown in Supporting Information Figure S5). These results are consistent with previous charcoal research [38,39].

3.3. Skeletal density trends

Biochar skeletal densities increased linearly (R^2 values > 0.93) with temperature (Fig. 2). For example, wood biochar skeletal density increased from 1.344 g cm^{-3} to 1.742 g cm^{-3} from 300 °C to 700 °C. This is consistent with other skeletal density

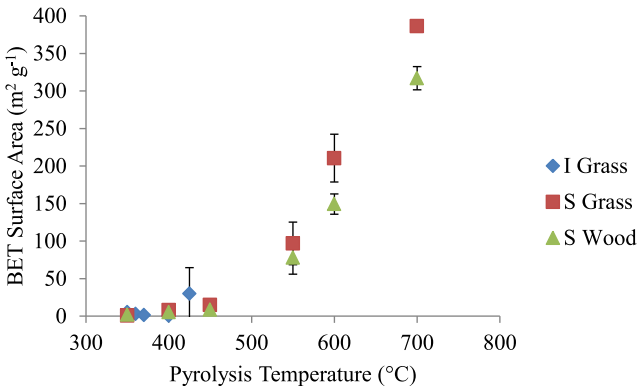

Fig. 1 – Biochar BET surface area as a function of pyrolysis temperature. S, slow pyrolysis; I, intermediate pyrolysis. Error bars represent 1 standard deviation, $n = 2$ for slow pyrolysis biochars 450–700 and I Grass 425.

Please cite this article in press as: Brewer CE, et al., New approaches to measuring biochar density and porosity, Biomass and Bioenergy (2014), http://dx.doi.org/10.1016/j.biombioe.2014.03.059

measurements of chars produced at different temperatures [18,40]. The increase with temperature is caused by the gradual condensation of carbon into aromatic clusters approaching graphite, which has a skeletal density of 2.25 g cm^{-3} [40], and the concentration of ash in the char product [18]. The increasing aromaticity with temperature is also supported by the decrease in molar H:C and O:C ratios (Table 1) [41]. Here, the feedstocks and biochars had similar ash contents, <70 g kg^{-1} on a dry basis. We attribute the variability in the skeletal density measurements (error bars in Fig. 2) primarily to the heterogeneity of the biochar samples, because the acceptable equilibrium variation on the pycnometer was set to <1 mm^3 cm^{-3} for five consecutive measurements (i.e. the pycnometer continues to repeat the analysis until five consecutive measurements have a standard deviation that is < 1 mm^3 cm^{-3} of the total measured volume for that sample aliquot).

3.4. *Envelope density and porosity trends*

Biochar envelope density varied substantially with feedstock: the wood biochars (at 0.47 g cm^{-3} to 0.6 g cm^{-3}) were denser than the grass biochars (0.25 g cm^{-3} to 0.3 g cm^{-3}, Fig. 3). Temperature and pyrolysis method appeared to have little to no effect on envelope density, although there was a slight trend towards decreasing density with increasing pyrolysis temperature for the wood biochars. Biochar porosities, calculated using Equation (1), ranged from 0.55 to 0.86. Porosity depended mostly on biochar feedstock (wood < grass) and increased slightly with pyrolysis temperature, but was not affected by pyrolysis method (Fig. 4). We attribute the difference in porosity between feedstocks to differences in cell shape and size distribution in woody and herbaceous plants, given that much of the original plant structure is maintained in the biochar after pyrolysis [12,16]. In addition, we speculate that the increase in porosity with temperature is caused by the progressive removal of volatiles from pores, and the physical and chemical condensation of the remaining skeletal structure with pyrolysis temperature.

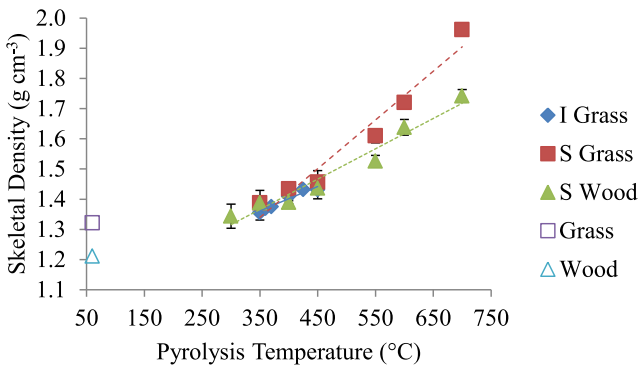

Fig. 2 – Skeletal density of biochars as a function of pyrolysis temperature and of feedstocks (dried at 60 °C). Linear fits: ρ_s S Grass = 0.0016*x* + 0.7735 (R^2 = 0.9539, dashed line), ρ_s S Wood = 0.001*x* + 1.0141 (R^2 = 0.9577, dotted line), ρ_s I Grass = 0.0008*x* + 1.0756 (R^2 = 0.9384, solid line). S, slow pyrolysis; I, intermediate pyrolysis. Error bars represent 1 standard deviation, *n* = 3.

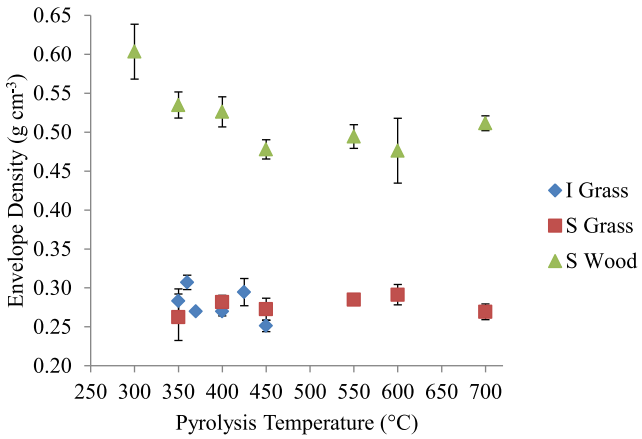

Fig. 3 – Envelope density of biochars as a function of pyrolysis temperature. S, slow pyrolysis; I, intermediate pyrolysis. Error bars represent 1 standard deviation, *n* = 3.

3.5. *Pore accessibility*

Skeletal density measurements made before and after grinding indicate that not all of the pores in our slow pyrolysis biochars were accessible to helium gas, and that pore accessibility only varied with pyrolysis temperature for the intermediate pyrolysis chars. For the slow pyrolysis chars, the relative skeletal density of ground biochars was higher than that of unground biochars, and significantly higher in some cases (Fig. 5). It should also be noted that the standard deviations for the unground biochar measurements were much higher than those for the ground biochars. This indicates that inaccessible porosity contributes to sample heterogeneity and that the best practice would be grinding of biochar prior to measuring skeletal density.

For the intermediate pyrolysis grass biochars, skeletal densities of the ground and unground I Grass 400 and I Grass 450 were the same (±0.01 g cm^{-3}). For I Grass 350, however, the skeletal density of ground biochar was significantly higher

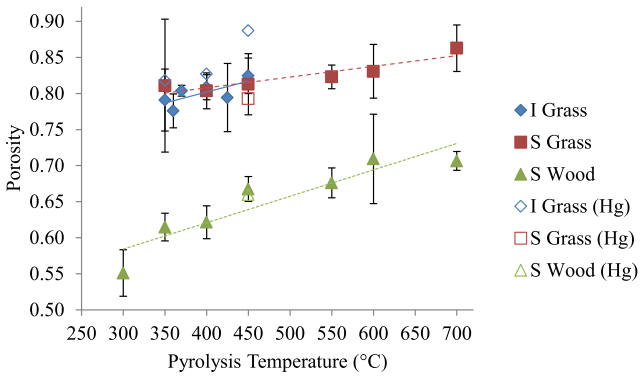

Fig. 4 – Porosity of biochars as a function of pyrolysis temperature as determined by pycnometry and mercury porosimetry (Hg). Linear fits: S Grass = 0.0001*x* + 0.7484 (R^2 = 0.8503, dashed line), S Wood = 0.0004*x* + 0.4743 (R^2 = 0.8529, dotted line), I Grass = 0.0003*x* + 0.6802 (R^2 = 0.521, solid line). S, slow pyrolysis; I, intermediate pyrolysis. Error bars represent 1 standard deviation, *n* = 3 for pycnometry.

Please cite this article in press as: Brewer CE, et al., New approaches to measuring biochar density and porosity, Biomass and Bioenergy (2014), http://dx.doi.org/10.1016/j.biombioe.2014.03.059

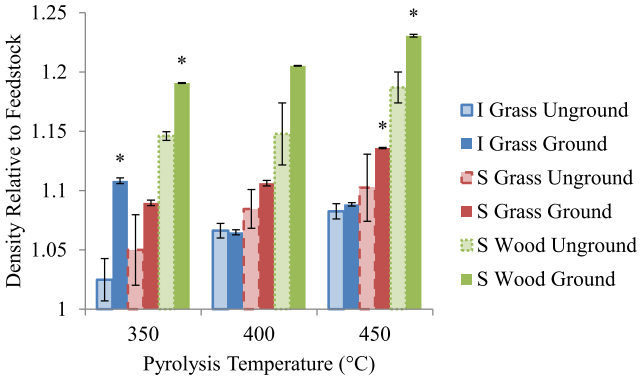

Fig. 5 – Skeletal density of ground (< 53 μm) and unground biochars relative to the skeletal density of the feedstock. S, slow pyrolysis; I, intermediate pyrolysis; *skeletal density of ground sample is significantly different than skeletal density of unground sample, $p < 0.05$. Error bars represent 1 standard deviation, $n = 3$.

than that of unground biochar (Fig. 5). This suggests that, at the lowest temperature, the incomplete pyrolysis reaction either did not rupture all of the plant cell walls through escaping volatiles or there was build-up of tars over the pore openings. The likelihood of incomplete pyrolysis is supported by the high O:C and H:C ratios compared to the slow pyrolysis biochars (Table 1).

3.6. *Pore size and characterization methodology*

Biochar pores span at least five orders of magnitude in size, with different size ranges relevant to different environmental processes. Consequently, careful consideration has to be given to the size ranges that different analysis methods can quantify (Fig. 6). For example, while biochar has been shown to have abundant pores in the nanometer size range that are important for chemical interactions [38], these pores are less relevant to questions of plant-available water, because plants are unable to exceed the high capillary forces holding water in extremely small pores.

In mercury porosimetry measurements of biochar, increases in pressure cause mercury to intrude into increasingly smaller pores. This makes it possible to plot apparent biochar density as a function of accessible pore size and thus retrieve some information about pore size distribution (Fig. S6). In general, the biochar densities measured by mercury porosimetry were comparable to those measured by pycnometry (Fig. 4). The mercury porosimetry skeletal density for I Grass 450, however, was substantially higher (1.91 g cm^{-3}) than that measured by He pycnometry (1.43 g cm^{-3}), resulting in a higher calculated total pore volume. Mercury porosimetry may, however, overestimate the total pore volume in biochar samples compared to pycnometry measurements because porosimetry detects both the spaces inside biochar particles and the spaces between biochar particles (intra- vs. inter-particle pores). Pycnometry, on the other hand, detects only the intra-particle pores.

Both mercury porosimetry and pycnometry measure much higher total pore volumes than nitrogen gas sorption (Fig. 7), because these methods are, in principle, capable of measuring all pores, as opposed to solely capturing micro-and meso-pores during gas sorption. It is noteworthy that biochar micro-pore volume and surface area were dependent primarily on pyrolysis temperature (Fig. S5), while macro-pore volume was primarily a function of biomass. This should be taken into account when trying to achieve specific pore size characteristics in biochars.

Compared to gas sorption, mercury porosimetry, or microscopy, pycnometry (the combination of skeletal density by helium pycnometry and envelope density by granular displacement) is a faster, cheaper, safer, and more effective technique for biochar total porosity measurements.

3.7. *Environmental implications*

Biochar physical properties such as particle size, density, and porosity, together with biochar chemical properties, are likely to determine the ecosystem services [2] provided by biochar amendment to soils. Density and porosity measurements are components in a suite of tools needed to understand both the short- and long-term effects of biochar addition to soils and biochar transport within the soil environment. The high porosity of the biochars in this study explains why many biochars will initially float when exposed to water even though their skeletal densities are greater than that of water. As water infiltrates air-filled biochar pores, the functional density gradually increases and the biochar may sink. The properties that control the transport kinetics of water into biochar pores are an essential next research step. Biochars with low envelope density, such as the miscanthus grass biochars, are more likely to float and be susceptible to preferential erosion during surface runoff. By the same token, biochars with high total pore volumes are more likely to increase soil water retention capacity. This suggests that amendment with grass biochars may increase soil water holding capacity more than wood biochars, although the lower envelope density of grass biochars may lead to more rapid erosion.

Porosity and pore connectivity may play a role in the accessibility of biochar's labile organic components for microbial enzymes, thus potentially enhancing the rapid mineralization rates observed initially after biochar soil amendment [42–44]. This labile fraction, which can account for a loss of 20 g kg^{-1} to 200 g kg^{-1} of biochar C, consists mainly of volatile organic compounds created during pyrolysis and condensed during cooling [45]. On the other hand, microporosity and high specific surface area have been suggested to play a role in the inhibition of the SOM mineralization after biochar application to soil. The underlying mechanism involves diffusion and sorption of organic matter constituents into the micropores, where they are physically protected against mineralization [45]. The ability to measure total pore volume by pycnometry, in combination with micro-pore measurement techniques, can be used to understand the relationship between biochar's pore size and pore volume, and soil nutrient cycling.

Tracking changes in biochar physical properties with environmental exposure will provide information on how biochar's effects on the ecosystem change over time. For

Please cite this article in press as: Brewer CE, et al., New approaches to measuring biochar density and porosity, Biomass and Bioenergy (2014), http://dx.doi.org/10.1016/j.biombioe.2014.03.059

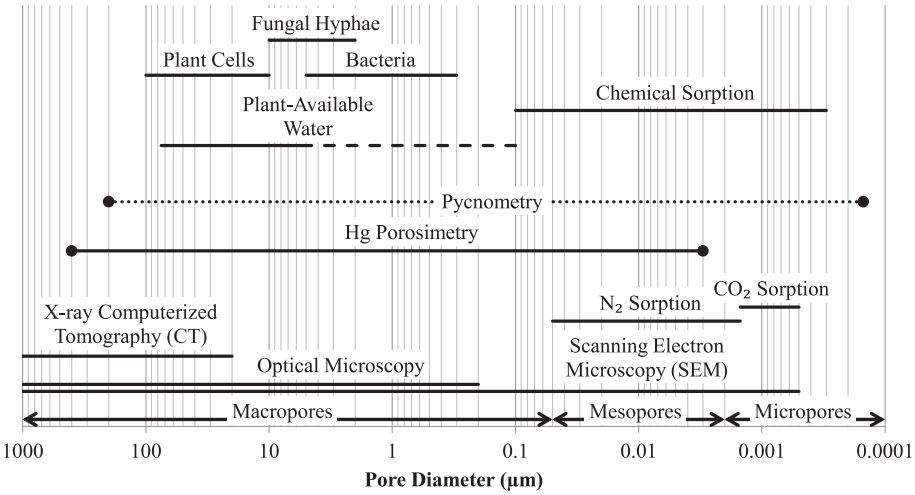

Fig. 6 – Pore size ranges by classification, analytical characterization techniques available, and relevant physiochemical phenomena for biochar interactions with the environment. Solid lines indicate methods that produce pore size distributions. Ranges framed by dots indicate methods that give cumulative pore volumes in that range. Plant-available water pore size range based on soil pore size classifications [47] (solid line) extended to pore sizes accessible if only capillary pressure is considered (dashed line).

example, infilling of biochar pores with microbes and clay minerals can be expected to increase biochar's density and decrease biochar's porosity, thereby affecting ecological and hydrologic properties. Changes in biochar porosity may also change the tensile strength of biochar-enriched soils, which has been identified as one mechanism promoting plant growth [46]. The next steps in biochar density and porosity studies should include the characterization of how porosity, pore-size distribution and density change as a consequence of exposure time and variations in agronomic practices, climate regimes, microbial ecology, and soil types.

4. Conclusions

Biochar physical properties are expected to play a key role in understanding how biomass feedstocks and pyrolysis conditions relate to biochar's environmental impacts. One challenge to characterizing the effects of biochar porosity on soil is reliable measurements of pore volume over the entire pore size range. In this study, we present an envelope density measurement technique that, when combined with skeletal density measured by helium pycnometry, can be used to estimate the total pore volume. This combined skeletal- and envelope-density analysis provides a novel and valuable method for quantifying biochar porosity characteristics at micro- to macro-pore scales. When applying this method to a variety of different biochars, we find that skeletal density and micropore volume are primarily controlled by pyrolysis temperature (reaction controlled), whereas envelope density, porosity, and macropore volume are predominantly a function of biomass anatomy (feedstock controlled).

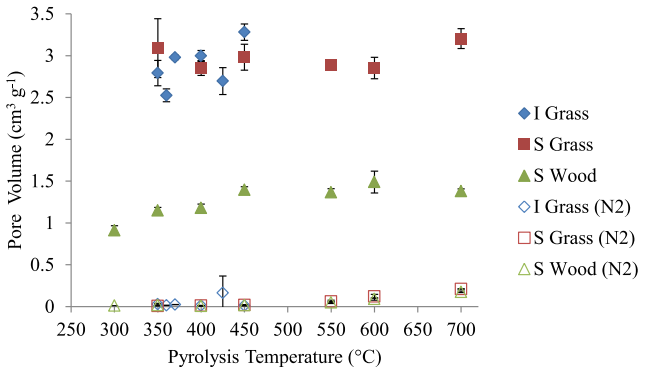

Fig. 7 – Total pore volume of biochars as a function of pyrolysis temperature as determined by pycnometry and nitrogen gas sorption (N2) at $P/P_0 = 0.995$ (N2 points are all located very close to the *x*-axis). S, slow pyrolysis; I, intermediate pyrolysis. Error bars represent 1 standard deviation, $n = 3$ for pycnometry and $n = 2$ for gas sorption.

Acknowledgments

The authors acknowledge funding from the Rice University Shell Center for Sustainability, from the European Community's Seventh Framework Programme ([FP7/2007-2013] under grant agreement n° 251492 awarded to C. A. Davies, and from Shell Global Solutions (UK). The authors also thank Mark Talarico of Micromeritics Analytical Services for his assistance with envelope density information and mercury porosimetry analyses, Dr. Tom Jones for his assistance with experimental design statistics, and anonymous reviewers for their helpful comments.

Appendix A. Supplementary data

Supplementary data related to this article can be found at http://dx.doi.org/10.1016/j.biombioe.2014.03.059.

REFERENCES

[1] Woolf D, Amonette JE, Street-Perrot FA, Lehmann J, Joseph S. Sustainable biochar to mitigate global climate change. Nat Comm 2010;1:56.
[2] Ecosystems and human well-being: synthesis. Washington, DC: Millenium Ecosystem Assessment; 2005. p. 137.
[3] Singh BP, Cowie AL, Smernik RJ. Biochar carbon stability in a clayey soil as a function of feedstock and pyrolysis temperature. Environ Sci Technol 2012;46(21):11770–8.
[4] Brockhoff SB, Christians NE, Killorn RJ, Horton R, Davis DD. Physical and mineral-nutrition properties of sand-based turfgrass root zones amended with biochar. Agron J 2010;102(6):1627–31.
[5] Warnock D, Lehmann J, Kuyper T, Rillig M. Mycorrhizal responses to biochar in soil – concepts and mechanisms. Plant Soil 2007;300(1):9–20.
[6] Rumpel C, Chaplot V, Planchon O, Bernadou J, Valentin C, Mariotti A. Preferential erosion of black carbon on steep slopes with slash and burn agriculture. Catena 2006;65(1):30–40.
[7] Rumpel C, Ba A, Darboux F, Chaplot V, Planchon O. Erosion budget and process selectivity of black carbon at meter scale. Geoderma 2009;154(1–2):131–7.
[8] Major J, Lehmann J, Rondon M, Goodale C. Fate of soil-applied black carbon: downward migration, leaching and soil respiration. Glob Change Biol 2010;16(4):1366–79.
[9] Masiello CA. New directions in black carbon organic geochemistry. Mar Chem 2004;92(1–4):201–13.
[10] Jaffe R, Ding Y, Niggemann J, Vahatalo AV, Stubbins A, Spencer RGM, et al. Global charcoal mobilization from soils via dissolution and riverine transport to the oceans. Science 2013;340:345–7.
[11] Dittmar T, Rezende CE, Manecki M, Niggemann J, Ovalle ARC, Stubbins A, et al. Continuous flux of dissolved black carbon from a vanished tropical forest biome. Nat Geosci 2012;5:618–22.
[12] Sun H, Hockaday WC, Masiello CA, Zygourakis K. Multiple controls on the chemical and physical structure of biochars. Ind Eng Chem Res 2012;51(9):3587–97.
[13] Downie A, Crosky A, Munroe P. Physical properties of Biochar. In: Lehmann J, Joseph S, editors. Biochar for environmental management science and technology. London: Earthscan; 2009.
[14] Keiluweit M, Nico PS, Johnson MG, Kleber M. Dynamic molecular structure of plant biomass-derived black carbon (biochar). Environ Sci Technol 2010;44(4):1247–53.
[15] Bird MI, Ascough PL, Young IM, Wood CV, Scott AC. X-ray microtomographic imaging of charcoal. J Archaeol Sci 2008;35(10):2698–706.
[16] Wildman J, Derbyshire F. Origins and functions of macroporosity in activated carbons from coal and wood precursors. Fuel 1991;70(5):655–61.
[17] Sing KSW, Everett DH, Haul RAW, Moscou L, Pierotti RA, Rouquerol J, et al. Reporting physisorption data for gas/solid systems with special reference to the determination of surface area and porosity. Pure Appl Chem 1985;57(4):603–19.
[18] Brewer CE, Schmidt-Rohr K, Satrio JA, Brown RC. Characterization of biochar from fast pyrolysis and gasification systems. Environ Prog Sustain Energy 2009;28(3):386–96.
[19] Nguyen BT, Lehmann J, Hockaday WC, Joseph S, Masiello CA. Temperature sensitivity of black carbon decomposition and oxidation. Environ Sci Technol 2010;44(9):3324–31.
[20] Lin Y, Munroe P, Joseph S, Henderson R, Ziolkowski A. Water extractable organic carbon in untreated and chemical treated biochars. Chemosphere 2012;87(2):151–7.
[21] Hao F, Zhao X, Ouyang W, Lin C, Chen S, Shan Y, et al. Molecular structure of corncob-derived biochars and the mechanism of atrazine sorption. Agron J 2013;105(3):773–82.
[22] Nocentini C, Certini G, Knicker H, Francioso O, Rumpel C. Nature and reactivity of charcoal produced and added to soil during wildfire are particle-size dependent. Org Geochem 2010;41(7):682–9.
[23] Martinez M, Torres M, Guzman C, Maestri D. Preparation and characteristics of activated carbon from olive stones and walnut shells. Ind Crop Prod 2006;23(1):23–8.
[24] Giesche H. Mercury porosimetry: a general (practical) overview. Part Part Syst Charact 2006;23(1):9–19.
[25] Illingworth J, Williams PT, Rand B. Characterisation of biochar porosity from pyrolysis of biomass flax fibre. J Energy Inst 2013;86(2):63–70.
[26] Weibel EW, Kistler GS, Scherle WF. Practical sterological methods for morphometric cytology. J Cell Biol 1966;30(1):23–38.
[27] Zygourakis K, Glass MW. Macropore size analysis using digital image-processing and a stereological model. Chem Eng Commun 1988;70(1):39–55.
[28] Mimmo T, Panzacchi P, Baratieri M, Davies CA, Tonon G. Effect of pyrolysis temperature on miscanthus (Miscanthus x giganteus) biochar physical, chemical and functional properties. Biomass Bioenergy 2014;62:149–57.
[29] Kinney TJ, Masiello CA, Dugan B, Hockaday WC, Dean MR, Zygourakis K, et al. Hydrologic properties of biochars produced at different temperatures. Biomass Bioenergy 2012;41:34–43.
[30] Sluiter A, Hames B, Hyman D, Payne C, Ruiz R, Scarlata C, et al. Biomass and total dissolved solids in liquid process samples. Golden, CO: National Renewable Energy Laboratory; 2008 March. p. 6. Report No.: NREL/TP-510-42621.
[31] Sluiter A, Hames B, Ruiz R, Scarlata C, Sluiter J, Templeton D. Determination of ash in biomass. Golden, CO: National Renewable Energy Laboratory; 2008 January. p. 5. Report No.: NREL/TP-510-42622.
[32] ASTM. Standard test method for chemical analysis of wood charcoal D1762-84. West Conshohocken, PA: ASTM International; 2007.
[33] Brewer CE, Hu Y-Y, Schmidt-Rohr K, Loynachan TE, Laird DA, Brown RC. Extent of pyrolysis impacts on fast pyrolysis biochar properties. J Environ Qual 2012;41(4):1115–22.
[34] Yang H, Yan R, Chen H, Zheng C, Lee DH, Liang DT. In-depth investigation of biomass pyrolysis based on three major components: hemicellulose, cellulose and lignin. Energy Fuels 2006;20(1):388–93.
[35] Maga JA. Polycyclic aromatic hydrocarbon (PAH) composition of mesquite (Prosopis fuliflora) smoke and grilled beef. J Agric Food Chem 1986;34(2):249–51.
[36] Brosse N, Dufour A, Meng X, Sun Q, Ragauskas A. Miscanthus: a fast-growing crop for biofuels and chemicals production. Biofuel Bioprod Biorefin 2012;6(5):580–98.
[37] Yang H, Yan R, Chen H, Lee DH, Zheng C. Characteristics of hemicellulose, cellulose and lignin pyrolysis. Fuel 2007;86(12–13):1781–8.
[38] Antal MJ, Gronli M. The art, science, and technology of charcoal production. Ind Eng Chem Res 2003;42(8):1619–40.
[39] Jimenez-Cordero D, Heras F, Alonso-Morales N, Gilarranz MA, Rodriguez JJ. Porous structure and morphology of granular chars from flash and conventional pyrolysis of grape seeds. Biomass Bioenergy 2013;54:123–32.
[40] Brown RA, Kercher AK, Nguyen TH, Nagle DC, Ball WP. Production and characterization of synthetic wood chars for

Please cite this article in press as: Brewer CE, et al., New approaches to measuring biochar density and porosity, Biomass and Bioenergy (2014), http://dx.doi.org/10.1016/j.biombioe.2014.03.059

use as surrogates for natural sorbents. Org Geochem 2006;37(3):321–33.
[41] McBeath AV, Smernik RJ, Schneider MPW, Schmidt MWI, Plant EL. Determination of the aromaticity and the degree of aromatic condensation of a thermosequence of wood charcoal using NMR. Org Geochem 2011;42(10):1194–202.
[42] Zimmerman AR. Abiotic and microbial oxidation of laboratory-produced black carbon (biochar). Environ Sci Technol 2010;44(4):1295–301.
[43] Smith JL, Collins HP, Bailey VL. The effect of young biochar on soil respiration. Soil Biol Biochem 2010;42(12):2345–7.
[44] Kuzyakov Y, Subbotina I, Chen H, Bogomolova I, Xu X. Black carbon decomposition and incorporation into soil microbial biomass estimated by ^{14}C labeling. Soil Biol Biochem 2009;41(2):210–9.
[45] Ameloot N, Graber ER, Verheijen FGA, De Neve S. Interactions between biochar stability and soil organisms: review and research needs. Eur J Soil Sci 2013;64:379–90.
[46] Chan KY, Van Zwieten L, Meszaros I, Downie A, Joseph S. Agronomic values of greenwaste biochar as a soil amendment. Aust J Soil Res 2007;45(8):629–34.
[47] Glossary of soil science terms. Madison, WI: Soil Science Society of America; 2008. p. 92.

Please cite this article in press as: Brewer CE, et al., New approaches to measuring biochar density and porosity, Biomass and Bioenergy (2014), http://dx.doi.org/10.1016/j.biombioe.2014.03.059